Electronic Supplementary Material (ESI) for Journal of Materials Chemistry C.

Enhancing $CsPbBr_3$ PeLEC properties by PDMS/PMHS double-layer polymer encapsulation and high relative humidity stress-aging

Maria Baeva, Anna S. Miroshnichenko, Ramazan Kenesbay, Dmitry M. Mitin, Vladimir V. Fedorov, Dmitry S. Gets, Dmitry V. Krasnikov, Albert G. Nasibulin, Sergey Makarov, Ivan S. Mukhin, Regina M. Islamova

Supporting Information

SI.1 Encapsulation Polymers Swelling Details

Swelling degree (*s*), soluble fraction (w_{sol}) and volume fraction (v) of PDMS (Sylgard 184) and AIBN-cured PMHS have been studied previously in literature and listed in **Table SI.1**.

Table SI.1. Swelling properties of PMHS and PDMS silicone rubbers in toluene at 120 °C.

Silicone rubber	*s*,%	w_{sol}, %	v	*Ref.*
PDMS (Sylgard 184)	190	4.1	0.48	[1]
PMHS	180	19	0.26	[2]

SI.2 Transparency of Annealed at 100 °C Nonencapsulated Perovskite Films

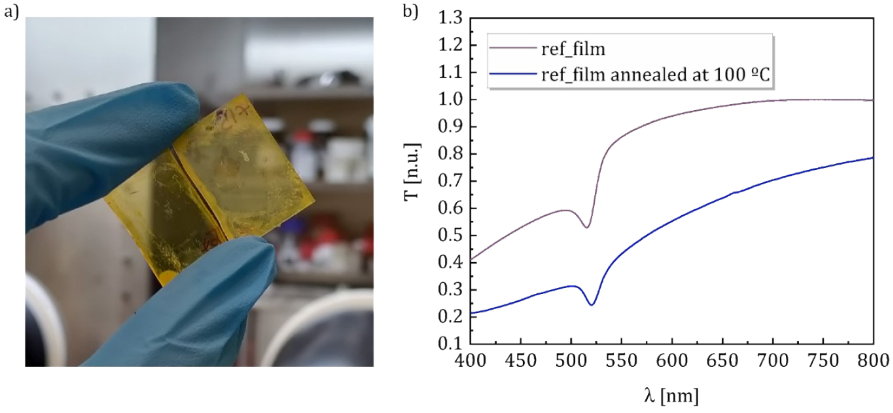

Figure SI.1 (a) Image of reference perovskite film (on the left) next to annealed at 100 °C non-encapsulated perovskite film (on the right) showcasing annealed film transparency loss; (b) Transmittance spectra of reference and annealed at 100 °C non-encapsulated perovskite film (all spectra were normalized to maximum of the reference film curve)

SI.3 Atomic Force Microscopy Details

Straightforward statistical parameters such as root-mean-square (RMS) surface roughness etc. are insensitive to lateral surface structure. We see that AFM image features of the reference film (see Figure SI.2a) and annealed film (see Figure SI.2c) are rather

different signifying distinctly different surface morphology. To quantitatively evaluate the difference in surface roughness in a comprehensive way we perform a standard power spectral density (PSD) analysis [3]. Derived 2-D PSD functions intensities (PSD functions intensities brightness is displayed in *log* scale for improved visualization) and their radially averaged surface roughness profiles are presented in Figure SI.2b, d and e, respectively. Obtained PSD function profiles illustrate how strong are height fluctuations at a given spatial frequency. It can be seen that spectral strength density over a range of spatial frequencies from 0.015 up to 0.15 nm^{-1} is more than an order of magnitude higher for the annealed film. Thus, we can conclude that overall, the surface of the annealed perovskite film becomes rougher, despite the formation of relatively flat areas in some regions.

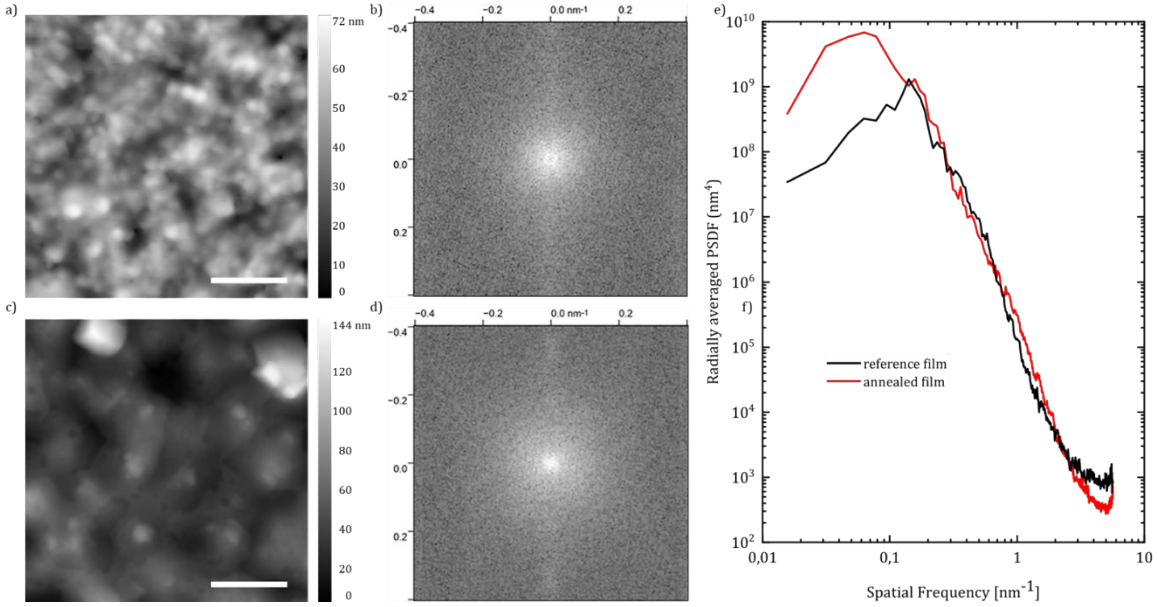

Figure SI.2 (a), (c) AFM images of reference and annealed (at 80 °C) films respectively; (b), (d) 2-D PSD functions intensities visualization of reference and annealed (at 80 ºC) films respectively; (e) radially averaged 2-D PSD profiles of reference and annealed (at 80 ºC) films. Scale bars in (a) and (c) images - 500 nm

SI.4 PL Images Digital Analysis Details

Density and size of non-photoluminescent domains were estimated using “Gwyddion” visualization and analysis software. Firstly, the original color PL images were converted into grayscale (GS) images, and after that, the GS images’ brightness maps were constructed. Areas of the images with low brightness (no photoluminescence) were marked with a red mask (see Figure SI.3) using the "Mark grains by threshold" tool. Then, we applied automatically generated by the “Gwyddion” statistical analysis to marked in red features. Table SI.2 shows the statistics for the reference and the annealed samples.

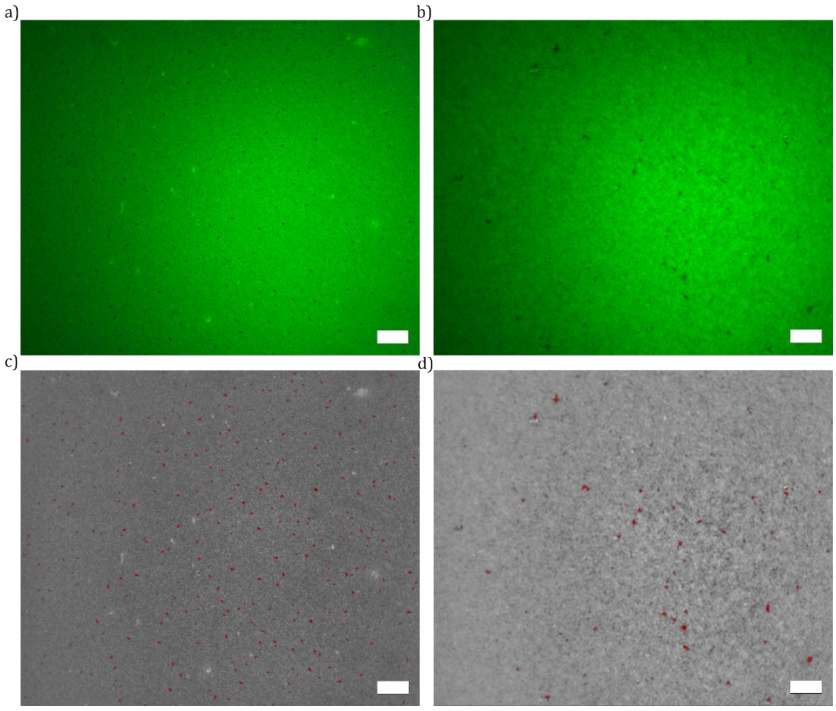

Figure SI.3 (a), (b) PL optical images of reference and annealed (at 80 °C) films respectively; (c), (d) GS images with red mask marked defects of reference and annealed (at 80 °C) films respectively. Scale bars in all images - 10 μm

Table SI.2 "Ref_film" and "a-ref_film" Samples' Parameters

Parameter	"ref_film"	"a-ref_film"
Non-photoluminescent domains	527	70
Density	3.39×10^{-2}	4.51×10^{-3}
Total non-photoluminescent domain area (relative) [%]	0.77	0.25
Average non-photoluminescent domain size [nm]	416	638

SI.5 Reference and Encapsulated Films Optical Images

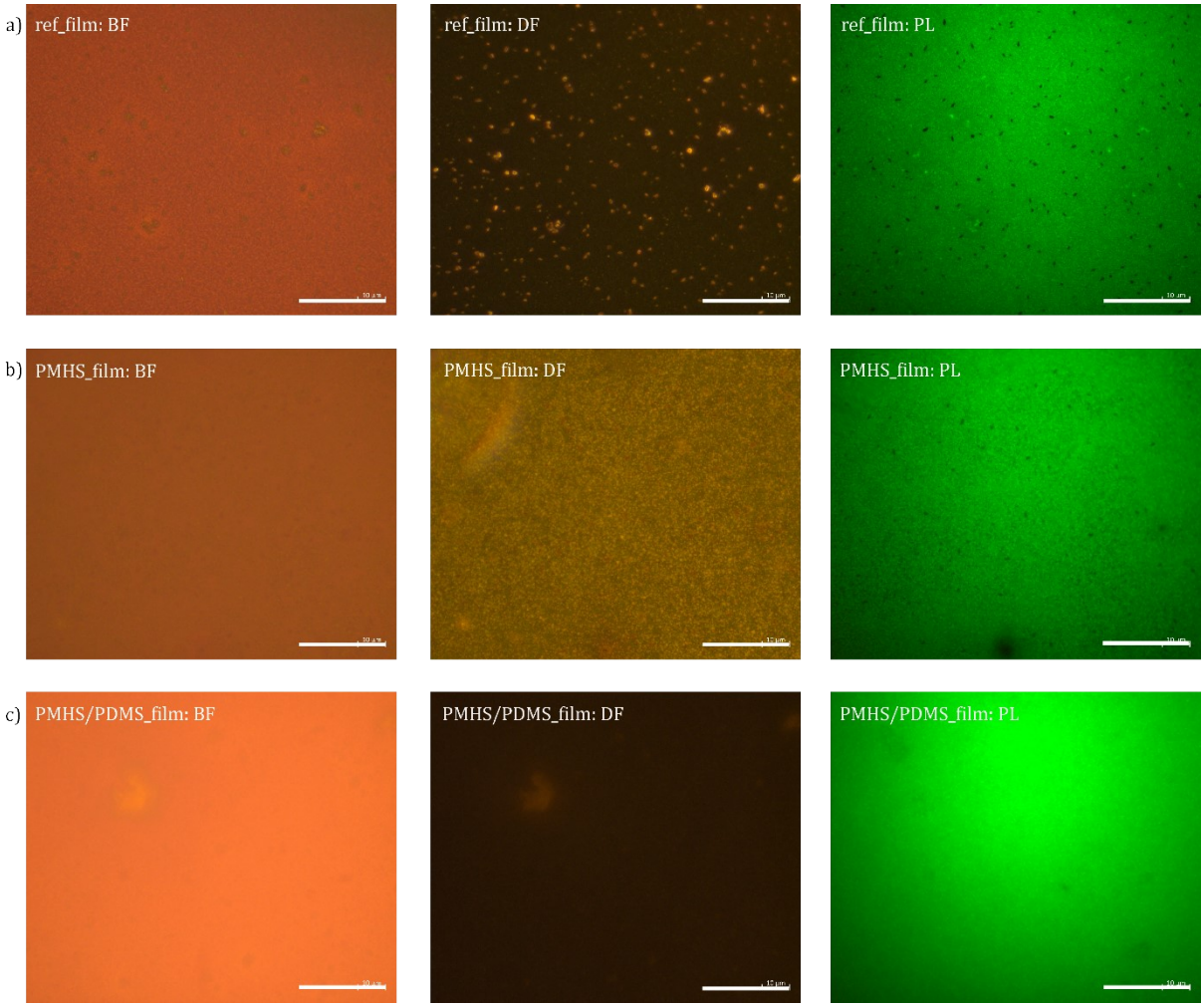

Figure SI4. (a) BF/DF/PL optical images of reference film; (a) BF/DF/PL optical images of PMHS encapsulated film; (a) BF/DF/PL optical images of PMHS/PDMS encapsulated film; Scale bars in all images - 30 µm

SI.6 Reflection from Double Encapsulation Layers

To evaluate the encapsulation polymer thickness on the perovskite film optical properties samples with various PMHS thicknesses were studied. The "Pink" sample was encapsulated into a single layer of 25 µm thick PMHS polymer; the "orange" sample – had two layers of 10 µm thick and 20 µm thick PMHS layers, see Figure SI.4.

Table SI3. Singe and Double PMHS Layers Encapsulation Details

Sample	PMHS thickness, µm
ref	N/A
single PMHS ("standard" PMHS)	~25
double PMHS ("thin" PMHS + "standard" PMHS)	~10 + ~25

Double PMHS PLQY in 50% higher than the reference sample PLQY, and twice as high as the films' encapsulated in a single PMHS layer. We associate that with the smoother film morphology, compared to the single-layer encapsulation: double-layer encapsulated films have less Rayleigh scattering contribution in the absorption spectra at $\lambda > \lambda_{absorption\ edge}$ (>525 nm).

The double-layer encapsulated perovskite films demonstrate less Rayleigh scattering alongside higher than single-layer encapsulated and reference samples – all points at higher material crystal structure quality when two stages of PMHS encapsulation are implemented.

To assess the polymer glassy surface influence on the possible light reflection we characterized the encapsulated and reference films' absorbance, and transmittance spectra from the front side (f, polymer/perovskite) and backside (b, glass). As expected, the deference film demonstrates higher absorption when incident light enters the film from the front side (perovskite), and the encapsulated films demonstrate higher absorption when incident light comes in from the back side (glass), especially, noticeable for λ_{inc} < 500 nm for the double-layer encapsulated film and over the whole wavelength range for the single-layer encapsulated film. This indicates that to a certain degree encapsulating polymer quenches incoming light somehow preventing it from entering the perovskite layer.

The reflectance spectra tell us that while the reference film is equally transparent when characterized from the front and from the back side, so is the double-layer encapsulated film: it demonstrates no discrepancy between transparency for front and back sides measurements. The single-layer encapsulated film is more transparent when measured from its back (glass) side than it is when it's measured from the front (polymer) side. The double-layer encapsulated film is more transparent than the single-layer encapsulated film at λ > 525 nm, which again indicates less "pronounced"/rough film morphology.

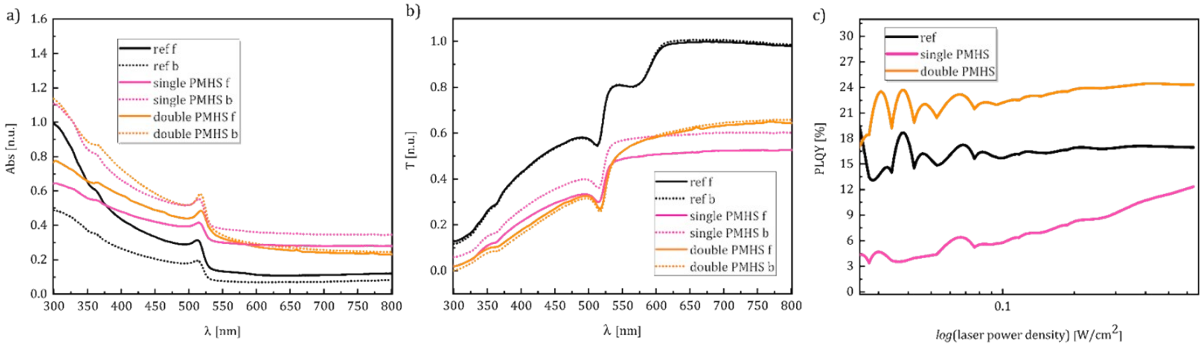

Figure SI.5 (a) Absorption spectra, (b) transmittance spectra, and (c) PLQY curves of reference, encapsulated in single- and double- layers perovskite films respectively (all spectra were normalized to ref film curve)

SI.7 Fourier-transform Infrared Spectroscopy Polymers Characterization Details

To study water penetration through polysiloxane capping layer into perovskite composites, a FTIR study was conducted for polysiloxanes films after 136 h aging at 80% RH (see Figure SI.5a) and for the reference film cured at room conditions (30-50% RH) (see Figure SI.5a). We observed no peak of -OH vibrations at 3200–3600 cm^{-1} in FTIR spectra which indirectly indicates the absence of water in all the films under study, even

after aging at 80% RH [4], [5]. The subsequent peaks at 2960 and 2903 cm $^{-1}$ could be assigned to -CH_3 (symmetric/asymmetric stretching) and -CH_2 (symmetric/asymmetric stretching) groups [6].

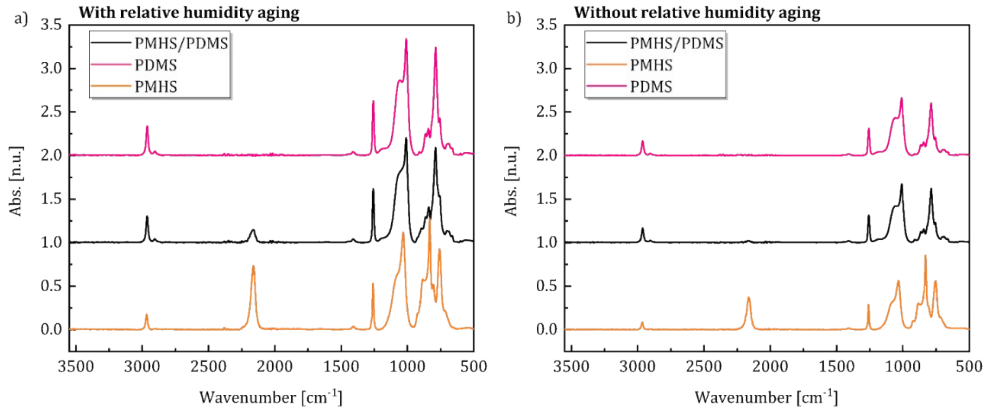

Figure SI.6 FTIR spectra of PDMS, PMHS, and PMHS/PDMS films (a) with and (b) without aging at 80% RH

Thus, we suggest the proposed encapsulation method helps to effectively isolate the perovskite composite from the influence of high humidity.

SI.8 *J-V* Curves for Nonencapsulated Annealed and Reference Devices

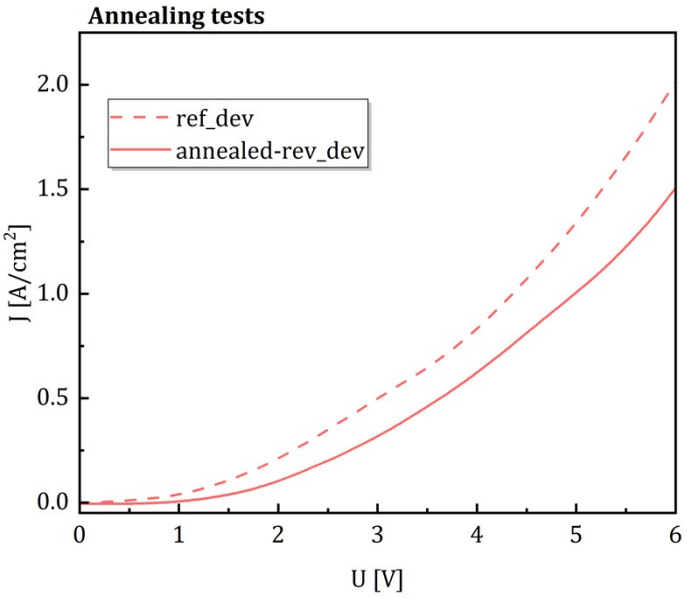

Figure SI.7 *J-V* curves for "ref_dev" and "a-ref_dev" samples

SI.9 XRD Characterization

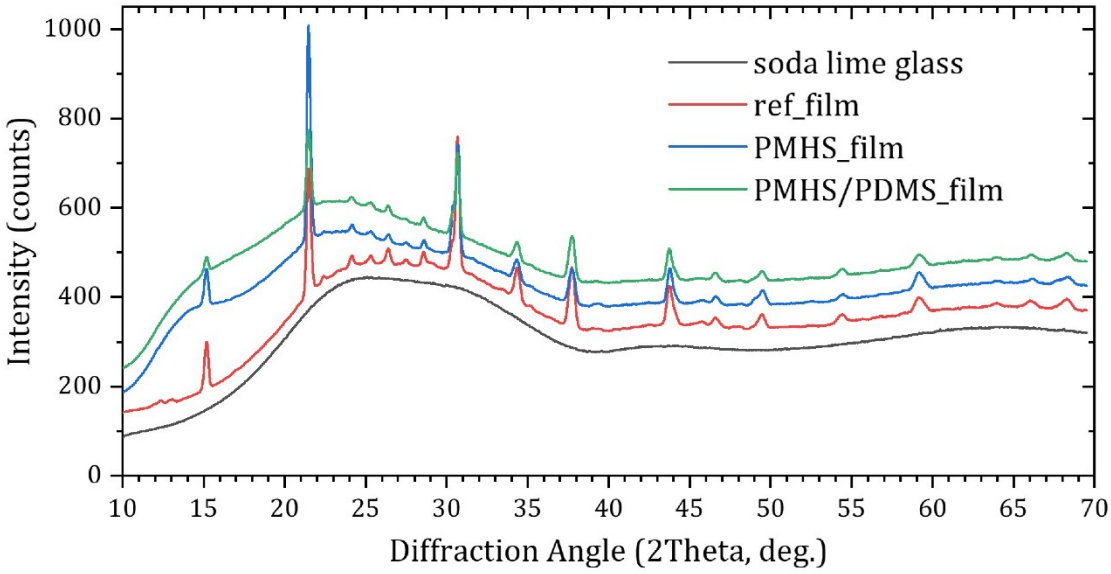

Figure SI.8. Raw XRD data. XRD curves are vertically shifted by 50 counts for clarity

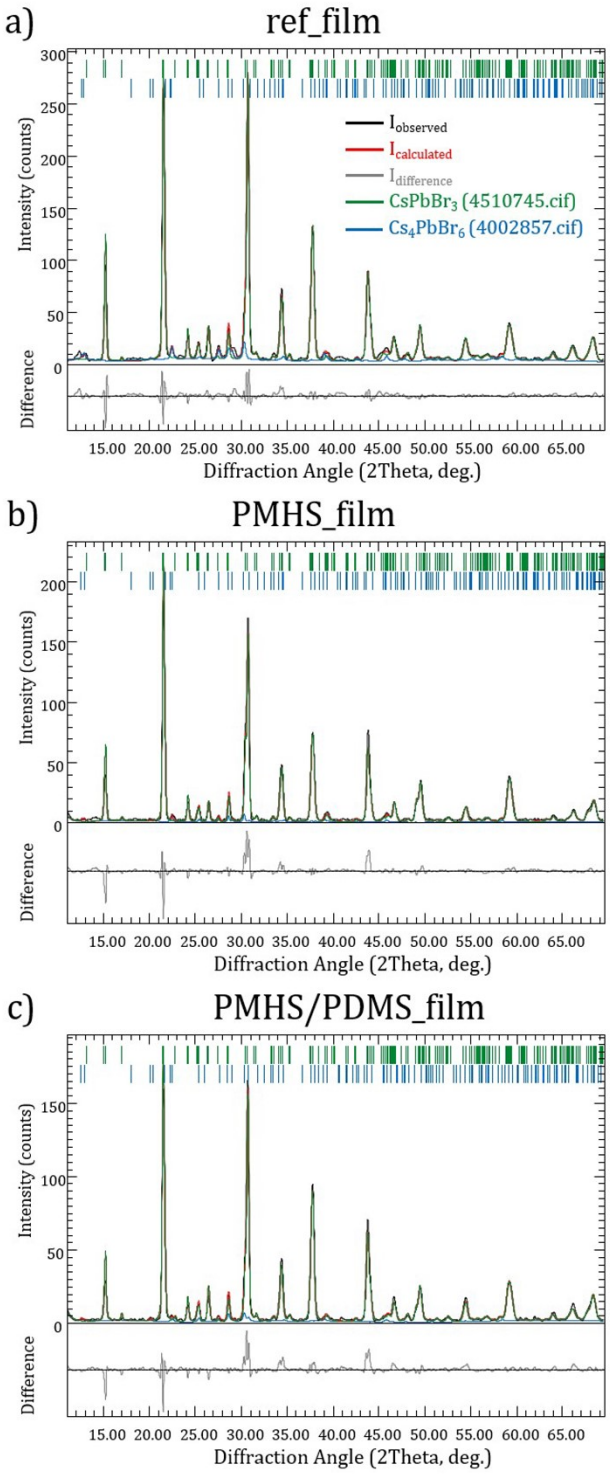

Figure SI.9. XRD phase analysis of perovskite thin films on glass. a) reference film, b) single (PMHS) and c) double (PMHS/PDMS) encapsulated films. Theoretical peak position for the CsPbBr3 (4510745.cif) and Cs4PbBr6 (4002857.cif) phases are shown by green and blue marks correspondingly

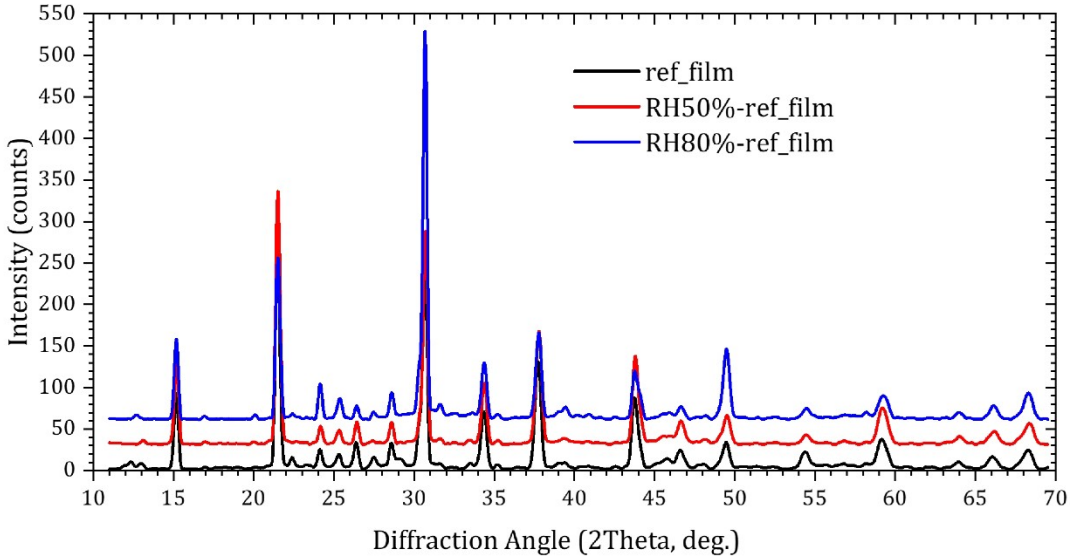

Figure SI.10. Effect of the RH treatment on the XRD pattern of the reference perovskite thin films on glass. Note the increase in the relative intensity of merged 220/004 Bragg peaks at 2Theta angle of 30.6 deg. Bragg peaks indicating the appearance of preferential orientation after the RH80% treatment

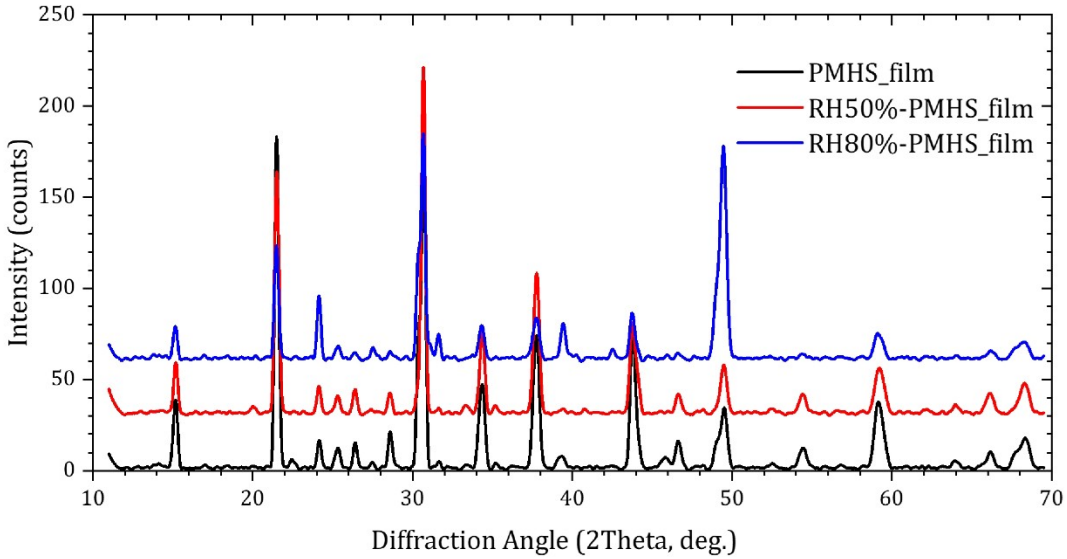

Figure SI.11. Effect of the RH treatment on the XRD pattern of the single encapsulated (PMHS) perovskite thin films on glass. Note the increase in the relative intensity of merged 240/420/332 Bragg peaks at 2Theta angle of 49.3 deg. And 220/004 Bragg peaks at 2Theta angle of 30.6 deg. indicating the appearance of preferential orientation after the RH80% treatment

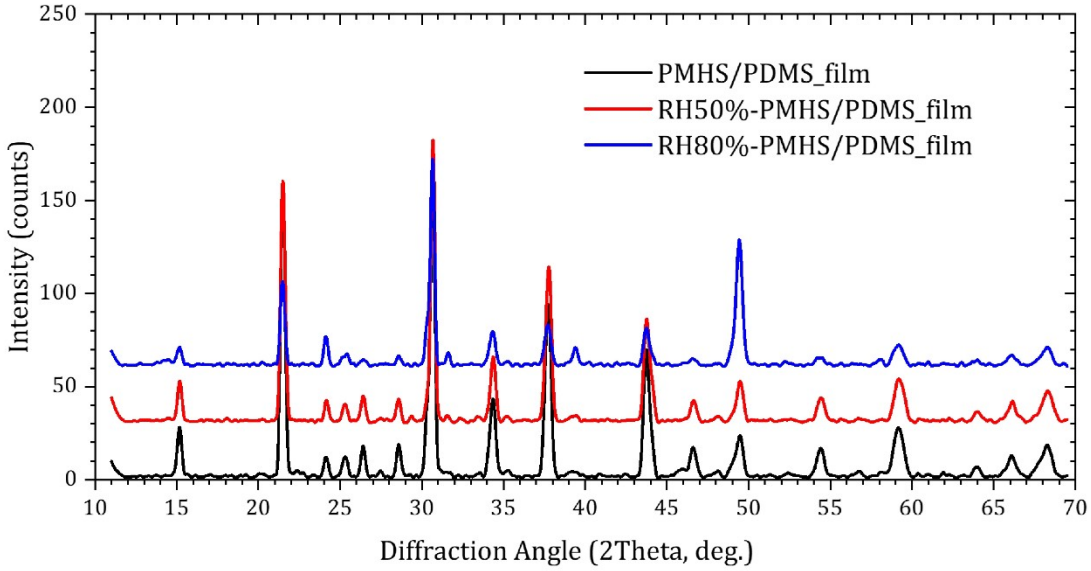

Figure SI.12 Effect of the RH treatment on the XRD pattern of the double encapsulated (PMHS/PDMS) perovskite thin films on glass. Note the increase in the relative intensity of merged 240/420/332 Bragg peaks at 2Theta angle of 49.3 deg. And 220/004 Bragg peaks at 2Theta angle of 30.6 deg. indicating the appearance of preferential orientation after the RH80% treatment

References

[1] A. S. Miroshnichenko *et al.*, "Flexible Perovskite CsPbBr 3 Light Emitting Devices Integrated with GaP Nanowire Arrays in Highly Transparent and Durable Functionalized Silicones," *J. Phys. Chem. Lett.*, vol. 12, no. 39, pp. 9672–9676, Oct. 2021.

[2] K. V. Deriabin, M. V. Dobrynin, and R. M. Islamova, "A metal-free radical technique for cross-linking of polymethylhydrosiloxane or polymethylvinylsiloxane using AIBN," *Dalt. Trans.*, vol. 49, no. 26, pp. 8855–8858, 2020.

[3] Y. Gong, S. T. Misture, P. Gao, and N. P. Mellott, "Surface Roughness Measurements Using Power Spectrum Density Analysis with Enhanced Spatial Correlation Length," *J. Phys. Chem. C*, vol. 120, no. 39, pp. 22358–22364, Oct. 2016.

[4] Y.-R. Kwon, J.-S. Kim, and D.-H. Kim, "Effective Enhancement of Water Absorbency of Itaconic Acid Based-Superabsorbent Polymer via Tunable Surface—Crosslinking," *Polymers (Basel).*, vol. 13, no. 16, p. 2782, Aug. 2021.

[5] A. S. Miroshnichenko *et al.*, "Lanthanide(III)-Incorporating Polysiloxanes as Materials for Light-Emitting Devices," *ACS Appl. Polym. Mater.*, vol. 4, no. 4, pp. 2683–2690, Apr. 2022.

[6] D. E. Kherroub, M. Belbachir, and S. Lamouri, "A new approach for the polymerization of tetraphenyltetramethylcyclotetrasiloxane by an environmentally friendly catalyst called Maghnite-H+," *Green Process. Synth.*, vol. 7, no. 4, pp. 296–305, Jul. 2018.